SUPPLEMENTARY INFORMATION

1. Radiative transfer

PACS and SPIRE observations of IRC +10216 have been obtained in November 2009[13]. The PACS data (55 – 200 μm) presented in the first paper describing the Herschel observations[13] were calibrated using a ground-based absolute flux calibration. Recently, a new absolute flux calibration for the PACS data has been obtained[12], yielding a decrease in absolute line flux of 30% in the blue wavelength range ($\lambda < 98\,\mu$m) and of 10% in the red wavelength range. The estimated calibration uncertainty on the PACS line fluxes is ∼30%, but is higher for wavelengths shortward of 63 μm due to non-optimal detector flatfielding. The PACS wavelength accuracy is around 20%[11]. For the SPIRE data (194 – 670 μm) the absolute flux calibration uncertainty is 15–20% between 194 and 313 μm, and 20–30% between 303 and 500 μm, going up to 50% beyond 500 μm.

These newly calibrated data (see Supplementary Figs. 1–5) have been used to rederive the thermal structure of the envelope around IRC +10216 through non-local thermodynamic equilibrium (non-LTE) radiative transfer modelling of the ^{12}CO lines, using the GASTRoNOoM code[26,31]. The PACS and SPIRE ^{12}CO lines cover energy levels from $J = 3$ (at 31 K) to $J = 47$ (at 5853 K) and trace the envelope for radii $r \lesssim 1 \times 10^{17}$ cm ($r < 2000\,R_\star$). The 60 lowest levels in the ground and first-vibrationally excited state are included in the radiative transfer modelling[26]. The velocity structure was obtained by solving the momentum equation. The (circum)stellar parameters are given in Table 1. Specifically, we derive a gas mass-loss rate of $2.1 \times 10^{-5}\,M_\odot$/yr for a [CO/$H_2$]-ratio of 1×10^{-3}[32] and a kinetic temperature that is given by $T(r) = T_{\rm eff}(R_\star) \times (r/R_\star)^{-0.58}$ (for $r < 10\,R_\star$) and $T(r) \propto r^{-0.4}$ beyond that radius. The estimated uncertainty on the mass-loss rate is a factor of 2. The derived kinetic temperature agrees very well with the results obtained for the inner envelope from a detailed modelling of C_2H_2 and HCN[33].

Using the derived thermodynamical structure, the level populations for ortho- and para-H_2O lines are calculated using the GASTRoNOoM-code for different stratifications of the water abundance throughout the envelope. The radiative transfer modelling includes the 45 lowest levels in the ground state and first vibrational state (i.e. the bending mode $\nu_2 = 1$ at 6.3 μm). Level energies, frequencies and Einstein A coefficients are extracted from the Barber water line list[34]. The H_2O-H_2 collisional rates are taken from the Faure database[35]. The effect of including excitation to the first excited vibrational state of the asymmetric stretching mode ($\nu_3 = 1$) has been tested, and is found to be negligible.

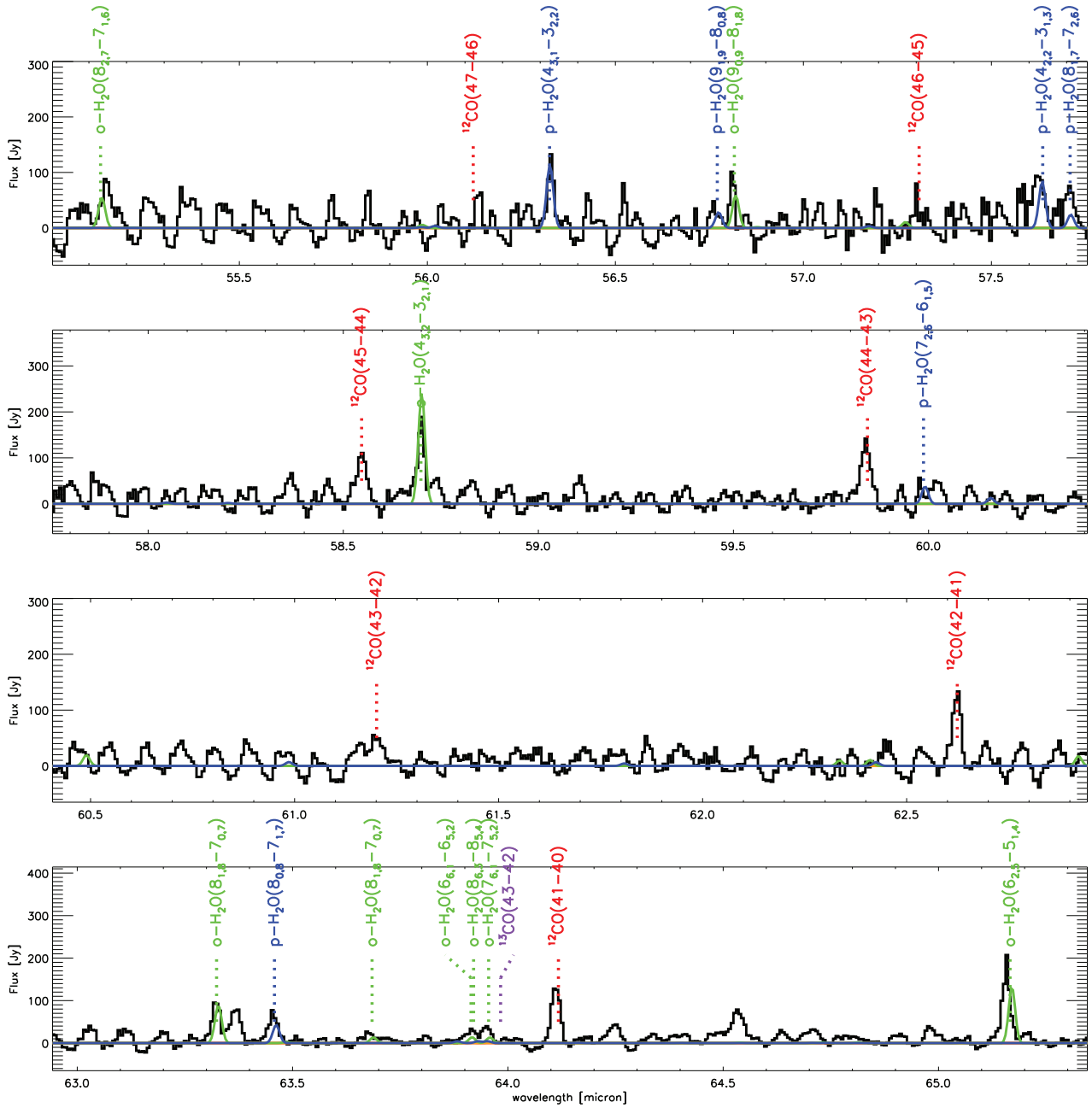

Supplementary Figure 1: **Herschel spectrum of IRC +10216 compared to water line predictions**. The Supplementary Figures 1–5 show the continuum subtracted Herschel PACS and SPIRE spectrum of IRC +10216 (in black). The coloured lines are the model predictions for ortho- and para-water with parameters as described in the caption of Fig. 1 in the main journal. The detected water lines and the ^{12}CO and ^{13}CO lines are indicated. In total, 39 ortho-water lines and 22 para-water lines are detected in the PACS and SPIRE spectrum. Most of the water lines seen in the Supplementary Figures 1–5 are blended with another molecular emission line arising from HCN, SiO, SiS, CO, etc.; a sub-sample of (almost) unblended water lines is presented in Fig. 1 in the main journal.

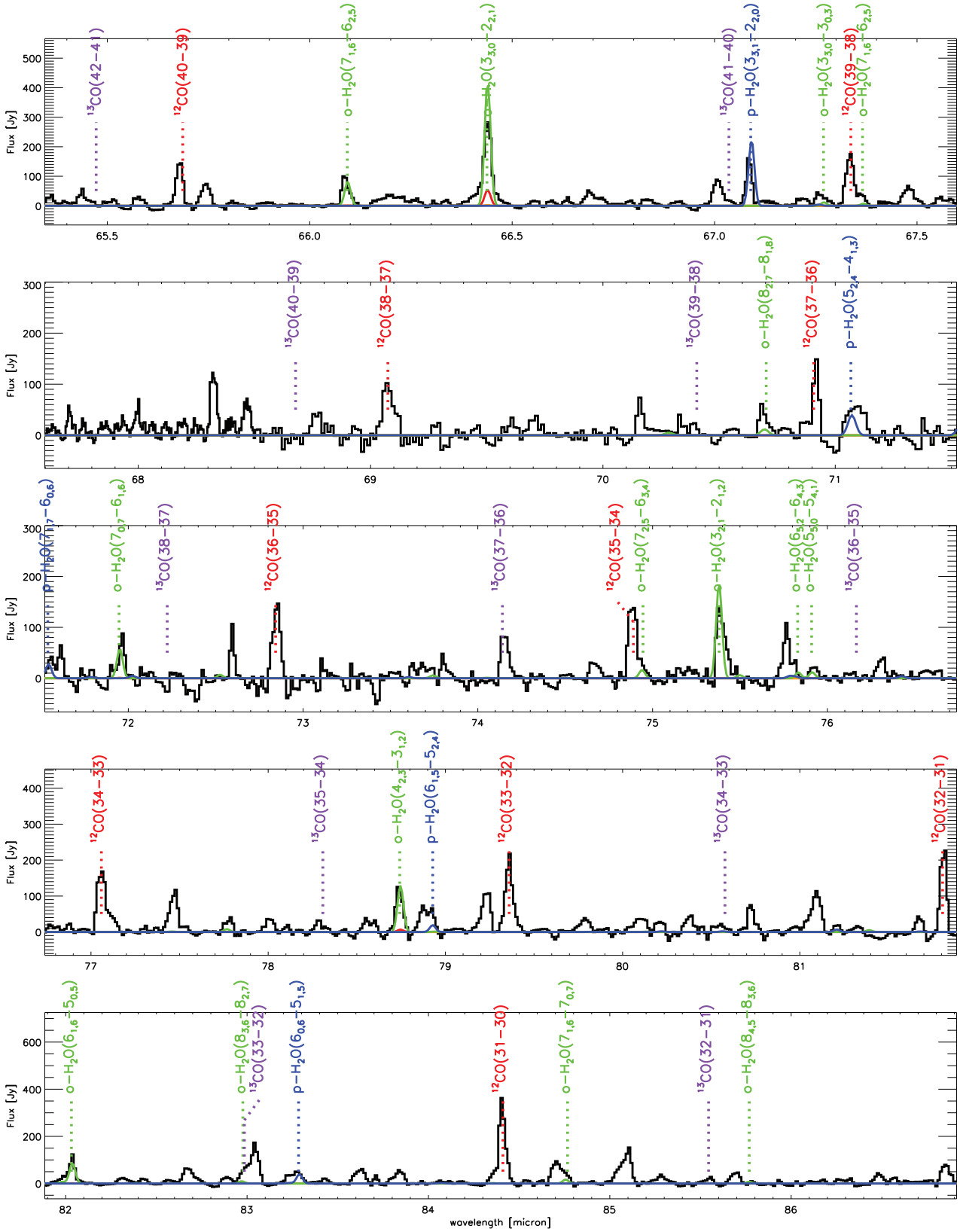

Supplementary Figure 2: see caption of the Supplementary Figure 1.

Supplementary Table 1: **(Circum)stellar parameters of IRC +10216.** $T_{\rm eff}$ is the effective stellar temperature, $R_\star$ denotes the stellar radius, v_∞ the terminal velocity of the wind, $\dot{M}$ the gas mass-loss rate, and $R_{\rm dust}$ the dust condensation radius.

$T_{\rm eff}$[K]	$2330^{(37)}$	$\dot{M}[M_\odot/{\rm yr}]$	2.1×10^{-5}
$R_\star$ $[10^{13}\,{\rm cm}]$	$5.1^{(38)}$	$R_{\rm dust}$ $[R_\star]$	$5.6^{(37)}$
$[{\rm CO/H_2}]$ $[10^{-3}]$	$1^{(32)}$	$^{12}{\rm CO}/^{13}{\rm CO}$	$30^{(13)}$
distance [pc]	$180^{(33)}$	v_∞ $[{\rm km\,s^{-1}}]$	$14.5^{(39)}$

Continuum emission provides the dominant excitation source for H_2O, mainly through absorption of $6\,\mu$m photons in the ν_2 band and subsequent decay[7]. The spectral energy distribution (SED) from $2\,\mu$m to 1 mm has been modelled using the MCMAX code[36], a radiative transfer code specialised for the treatment of optically thick dusty circumstellar media. The relevant stellar and circumstellar input parameters are identical to the ones used in the molecular emission line modelling. The best fit to the ISO SWS and LWS (Infrared Space Observatory, Short Wavelength Spectrometer and Long Wavelength Spectrometer) spectrophotometric data between 2.4 and $197\,\mu$m, supplemented with photometric data points[40], requires the inclusion of amorphous carbon, iron, silicon carbide and magnesium sulfide as dust species. Assuming spherical grains, their respective derived mass fraction abundances are 0.72, 0.05, 0.13 and 0.10. From these relative abundances, the mean specific density of the dust grains, the dust mass-loss rate and the wavelength-dependent absorption efficiencies are calculated to provide the dust component during the modelling of the molecular emission lines. The derived dust mass-loss rate is $8\times10^{-8}\,M_\odot$/yr, yielding a dust-to-gas ratio of $\sim 4\times10^{-3}$. Estimated uncertainties are a factor of 2. The mean specific dust density is $2.41\,{\rm g\,cm^{-3}}$.

The water fractional abundance as derived from the SWAS observations (see Fig. 2) is slightly higher than results presented already in the literature[7]. This mainly reflects a difference

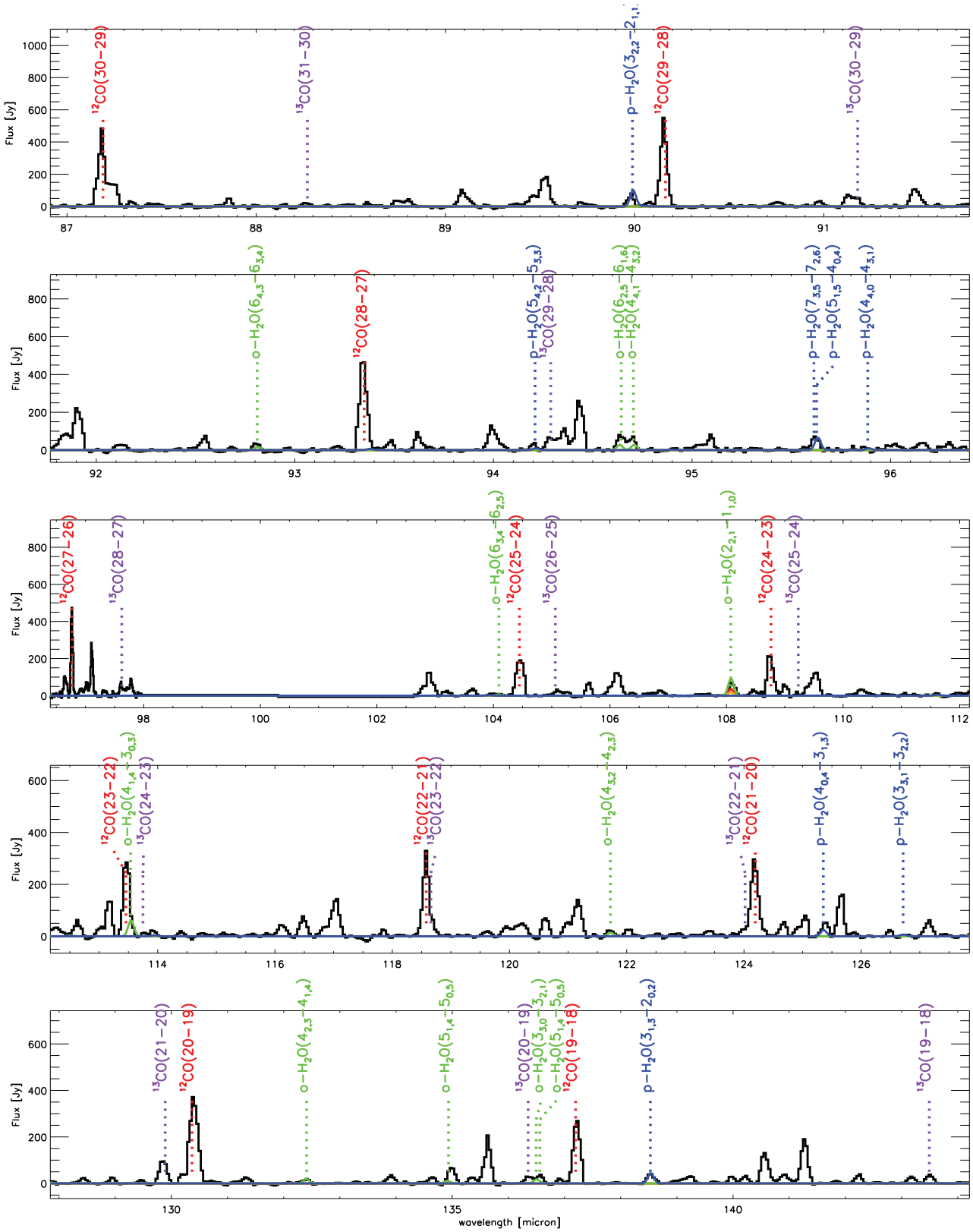

Supplementary Figure 3: see caption of the Supplementary Figure 1.

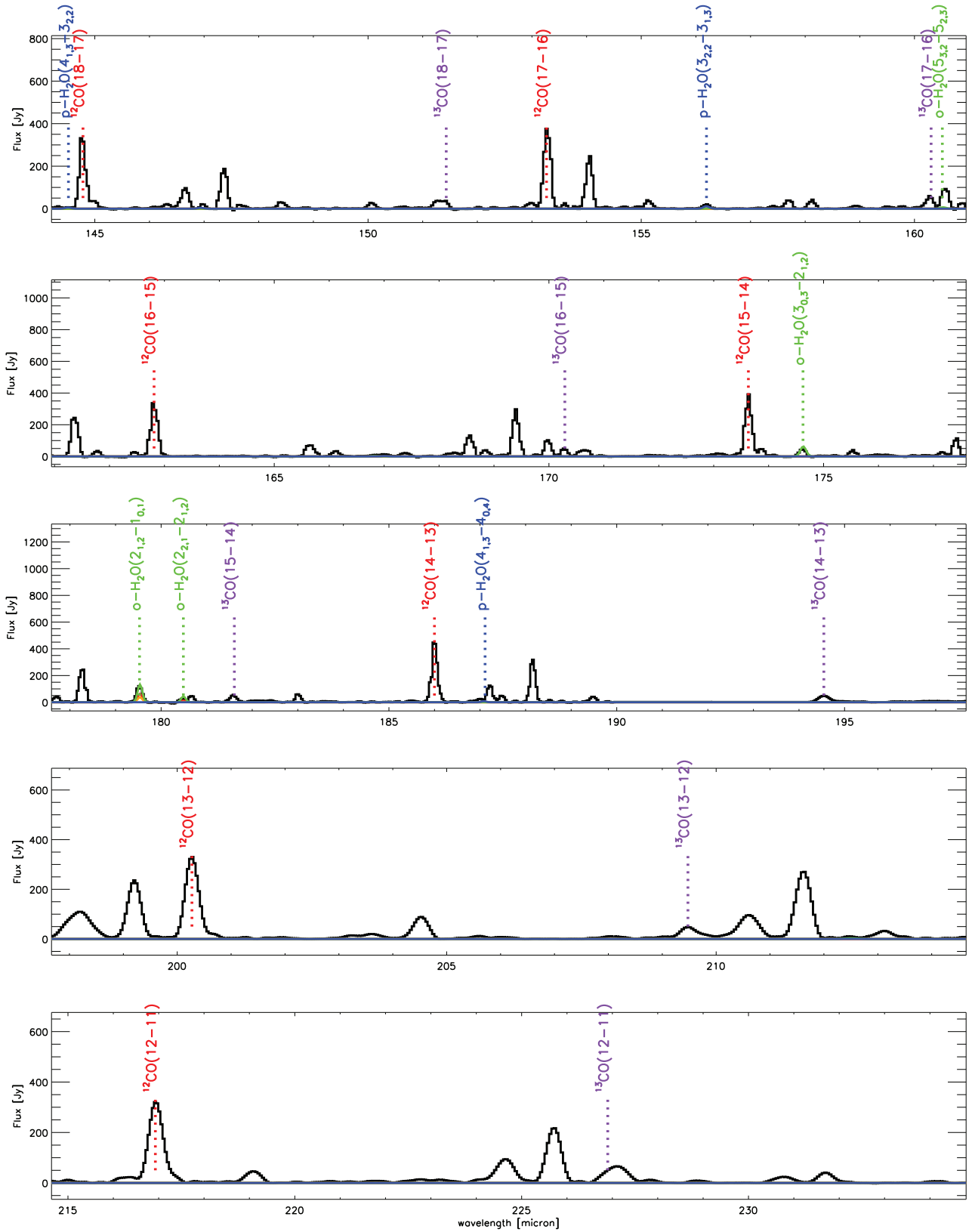

Supplementary Figure 4: see caption of the Supplementary Figure 1.

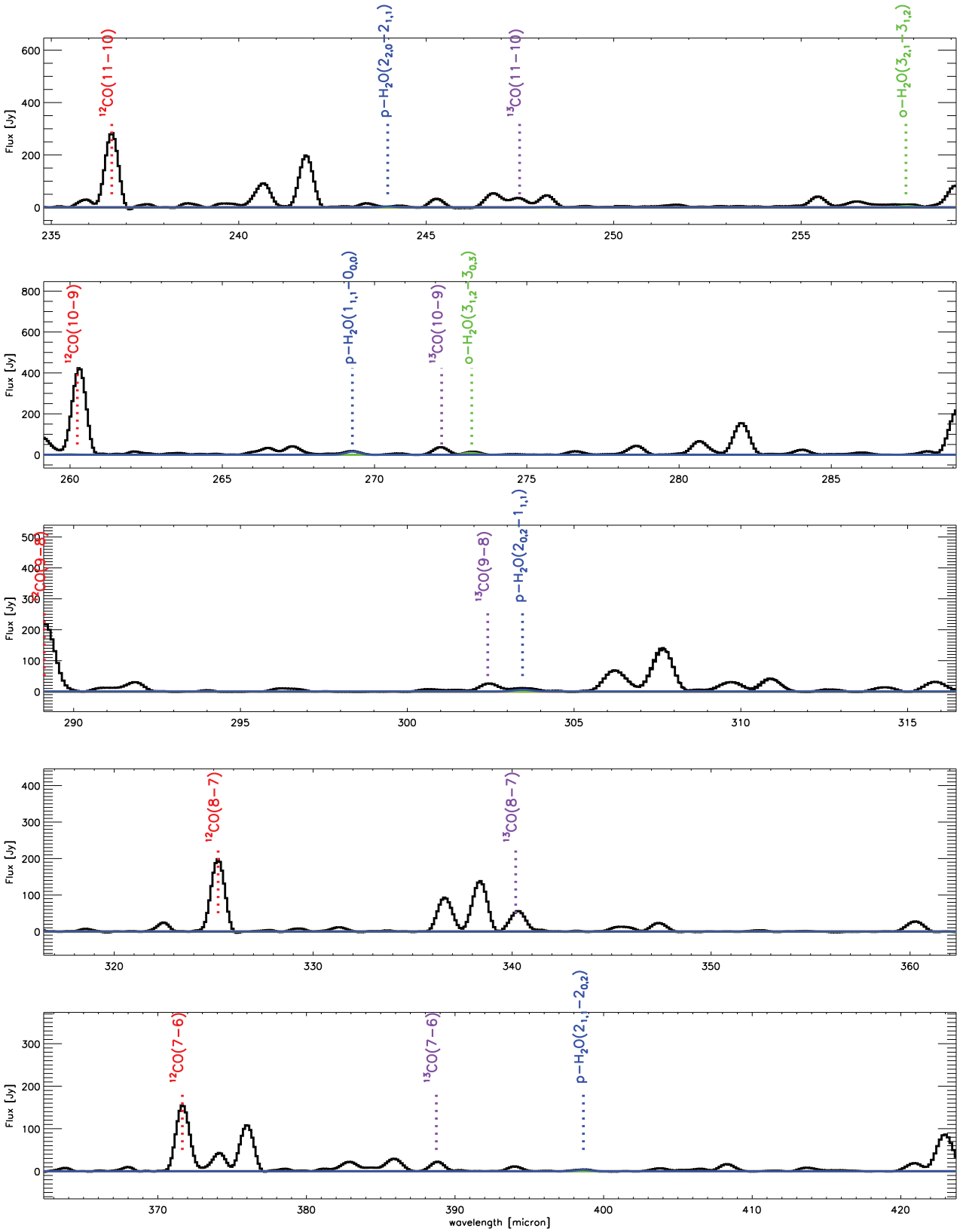

Supplementary Figure 5: see caption of the Supplementary Figure 1.

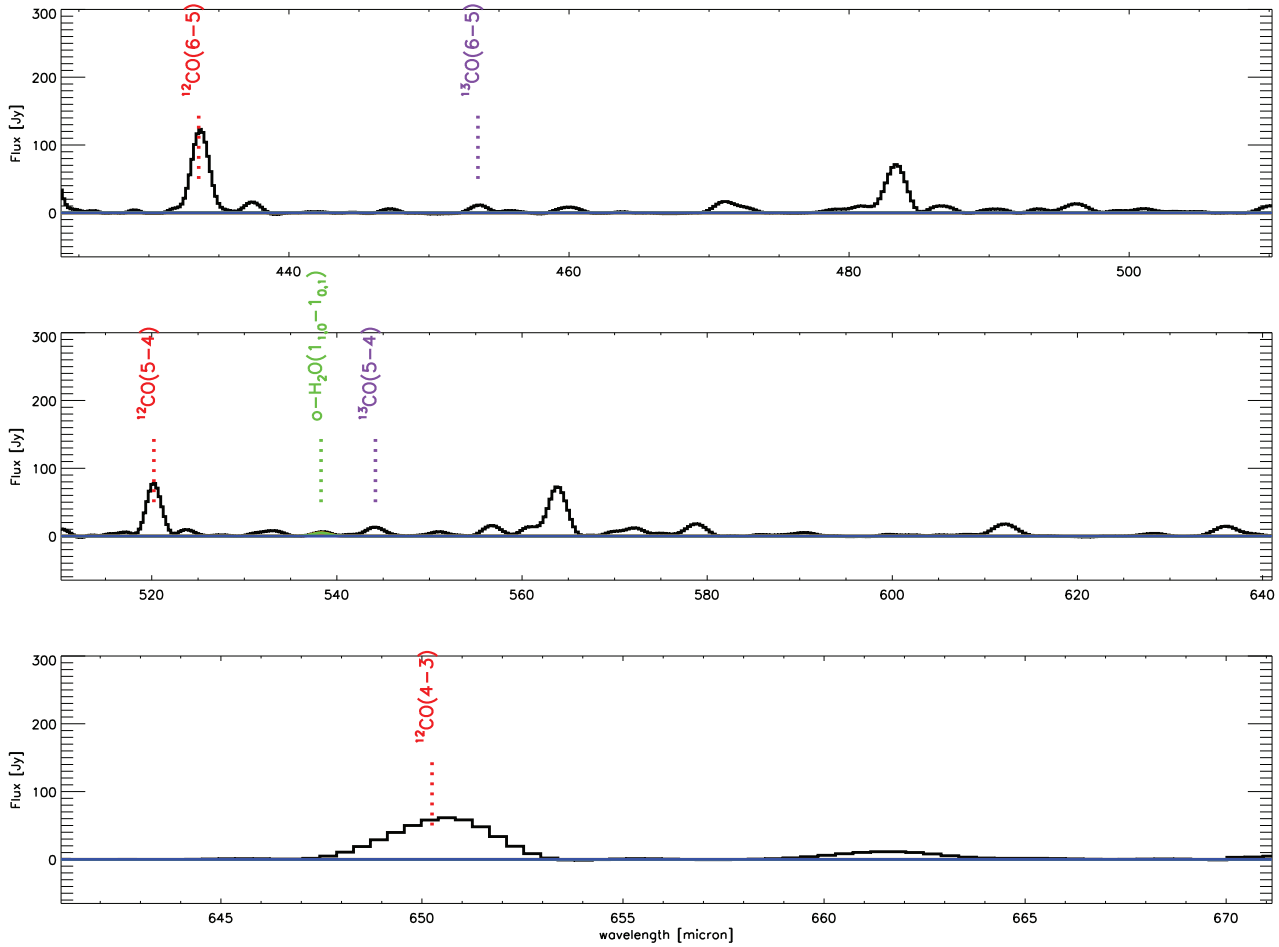

Supplementary Figure 6: see caption of the Supplementary Figure 1.

in (circum)stellar parameters and dust opacities. Using the same input parameters, similar abundances are derived.

2. Chemical modelling

There is a lot of evidence for a clumpy structure of the envelope around IRC +10216 from astronomical observations carried out at small and large scales in the visible and near-infrared wavelength ranges[29,30]. These optical and near-infrared observations trace the dust density distribution, and thus the gas density distribution if both dust and gas are position coupled[17]. Millimetre-wave interferometric observations have mapped the spatial distribution of CO, finding a large scale clumpy structure[16]. Other molecules, such as CN, C_2H, C_4H, and HC_5N show a clumpy and hollow quasi-spherical distribution with a lack of molecular emission in the NNE to SSW direction[17,18]. The hollow distribution can be interpreted in terms of photochemistry

of the parent species, creating reactive species which then undergo further chemical reactions[41]. The conical holes in the NNE and SSW directions have been interpreted in terms of a molecular density minimum in that part of the envelope[12], or the fact that IRC +10216 is just leaving the AGB and that a bipolar outflow has dug out two symmetric conical holes at a position angle PA$\sim$20°[42]. The existence of these clumps and conical holes opens a path for interstellar UV photons to penetrate deep into the envelope.

Whilst the existence of clumpy structures and cavities in the envelope of IRC +10216 is not in doubt according to the observations, it is difficult to model this complicated structure, since the different parameters characterizing the three-dimensional clumpy structure are not well constrained by the observations. We have thus adopted a simple modelling approach to simulate the clumpy structure and to investigate the effects on the circumstellar chemistry. We considered that the envelope consists of two different components: a major one which is well shielded against interstellar UV photons and only starts to undergo photochemistry in the outer layers, and a minor one (which accounts for a fraction f_M of the total circumstellar mass) for which the shielding material located in the radial outward direction is grouped into clumpy structures leaving a fraction f_Ω of the solid angle of arrival of interstellar light free of matter. We name these two components 'the major UV-shielded' and 'the minor UV-illuminated' component. As might be clear the minor UV-illuminated component is not completely exposed to UV photons, but is also partially shielded against UV photons by the clumps located on the way to the interstellar medium. Likewise, the major UV-shielded component starts to be partially exposed to UV photons in the outer envelope.

The physical conditions in both components are assumed to be the same, except that for the minor UV-illuminated component the visual extinction against interstellar light is reduced, as compared to that of the major UV-shielded component, due to the empty space between the clumpy material. The observations quoted in the previous paragraph have not provided an estimate of the density in the interclump medium. In our chemical model we have assumed that the density in the interclump medium is formally zero (in practice it is low enough to allow interstellar UV photons to penetrate without significant extinction). The clumpiness is assumed to extend down to the innermost regions of the envelope ($r \sim 10^{14}$ cm). Therefore, besides the standard physical parameters of any model describing a spherical circumstellar envelope (see Supplementary Table 1), we utilize two further phenomenological parameters to take care of the effects of clumpiness on the chemistry: for the minor UV-illuminated component f_M is the fraction of the total circumstellar mass in the minor component and f_Ω is the fraction of the solid angle of arrival of interstellar light which is free of matter.

The gas phase chemical composition of both the major UV-shielded and the minor UV-illuminated components are obtained from chemical kinetic calculations starting at the innermost layer ($r = 10^{14}$ cm) up to a distance of $r = 10^{18}$ cm, where most molecules have already been destroyed by interstellar UV photons. The chemical network utilized is essentially that

used in previous work on the chemistry of oxygen in IRC +10216[4], with updates for some reaction rate constants and photodissociation/ionization rates from the recent literature[43, 44]. The interstellar UV field has been decreased by a factor of 2 with respect to the standard interstellar UV field[45], to predict the angular position of the maximum abundance of C_2H and CN at 15″ and 20″ from the star, respectively, in agreement with interferometric observations[46]. We note that when fitting the peak abundance distribution of these molecules, there exists a degeneracy between various physical parameters, such as the interstellar UV field, the mass loss rate, the extinction law, and the distance to IRC +10216. Furthermore, the exact value of the local interstellar UV field around IRC +10216 is not precisely known. Recently, an extended UV structure surrounding IRC +10216 has been discovered at a radial distance of about 12′[47]. This structure has been attributed to the interaction of the stellar wind with the interstellar medium, and it might contribute to the ambient UV field seen by the circumstellar envelope of IRC +10216. The exact value of the interstellar UV field around IRC +10216 is, however, not critical in determining the flux of UV photons reaching the inner layers of the minor UV-illuminated component. What really counts is the degree of clumpiness, i.e. the parameter f_Ω. A more detailed description of the chemical modelling approach for this kind of environment, with a major UV-shielded and a minor UV-illuminated component, for both carbon- and oxygen-rich circumstellar envelopes with different mass-loss rates will be presented in another article[24].

For the envelope around IRC +10216, the inner regions of the major UV-shielded component (surrounded by a smooth envelope) are indeed well shielded against interstellar UV photons, with a visual extinction larger than 50 mag for the regions down to $5\,R_\star$[46]. Assuming that the minor UV-illuminated component is illuminated by interstellar UV photons in a cone where matter is just filling 50–80% of the solid angle of arrival of interstellar light ($f_\Omega = 0.5$–0.2), results in a substantial decrease of the effective visual extinction in the inner envelope from more than 50 mag to less than 0.5 mag, which indeed allows for photochemistry to take place in the inner envelope. In the final model, whose results are shown in Fig. 3 of the main article, we have adopted a value of 0.3 for f_Ω and assumed that the minor UV illuminated component accounts for 10% of the total circumstellar mass ($f_M = 0.1$). The resulting abundance radial profile for each species i are then obtained as the weighted-average of the abundance in both components, i.e. as $\overline{X_i}(r) = (1 - f_M)X_i^{\rm major}(r) + (f_M)X_i^{\rm minor}(r)$, where $X_i^{\rm major}(r)$ and $X_i^{\rm minor}(r)$ are the abundance of the species i in the major UV-shielded and minor UV-illuminated component, respectively, as a function of radius r. This approach assumes that the major UV-shielded and the minor UV-illuminated components are not distributed over a given preferred radial direction but over many different radial directions, in such a way that we can average over all directions to get a mean value of the abundance $\overline{X_i}$ at each radius r. Whilst it is clear that in reality both components cannot coexist in the same radial directions, this approach permits us to describe the distribution of the molecular abundances under spherical geometry, which facilitates the radiative transfer modeling described in Sect. 1. We note that the effect of a clumpy medium on spectral line formation can be characterized by a single number multiplying

the mean column opacity[48]. Even for an arbitrarily complex clump distribution, the effect can be reduced to a single scaling number. The scaling factor reduces the effective opacity of a clumpy medium compared to a smooth gas of the same mean column density. The scaling factor is directly retrieved from the chemical modelling (see Fig. 3 in the main article) and taken into account when modelling the H_2O line profiles.

As shown in Fig. 3 of the main article, water vapour reaches a weighted-averaged abundance relative to H_2 in excess of 10^{-7}. The photodissociation radius for each molecule is calculated from the chemical network taking the two components into account. According to the model water extends from the innermost regions ($r \sim 10^{14}$ cm) up to a radial distance of (1–3) $\times$ 10^{16} cm. In this region water vapour keeps a roughly constant abundance due to the balance between the formation processes (the reaction of O and H_2 followed by that of OH and H_2) and the destruction processes (photodissociation by the ambient interstellar UV field). The photodissociation radius of water, (1–3) $\times$ 10^{16} cm, is noticeably lower than that predicted by other hypotheses, 4×10^{17} cm (see main article). The smaller photodissociation radius obtained by our model is fully consistent with the SWAS, PACS, and SPIRE observations, as shown in Fig. 2 of the main article.

References

31. Decin, L. *et al.* Probing the mass-loss history of AGB and red supergiant stars from CO rotational line profiles. I. Theoretical model - Mass-loss history unravelled in VY CMa. *A&A* **456**, 549–563 (2006).

32. Zuckerman, B. & Dyck, H. M. Carbon monoxide emission from stars in the IRAS and revised AFGL catalogs. I - Mass loss driven by radiation pressure on dust grains. *ApJ* **304**, 394–400 (1986).

33. Fonfría, J. P., Cernicharo, J., Richter, M. J. & Lacy, J. H. A Detailed Analysis of the Dust Formation Zone of IRC +10216 Derived from Mid-Infrared Bands of C_2H_2 and HCN. *ApJ* **673**, 445–469 (2008).

34. Barber, R. J., Tennyson, J., Harris, G. J. & Tolchenov, R. N. A high-accuracy computed water line list. *MNRAS* **368**, 1087–1094 (2006).

35. Faure, A. *et al.* Quasi-classical rate coefficient calculations for the rotational (de)excitation of H_2O by H_2. *A&A* **472**, 1029–1035 (2007).

36. Min, M., Dullemond, C. P., Dominik, C., de Koter, A. & Hovenier, J. W. Radiative transfer in very optically thick circumstellar disks. *A&A* **497**, 155–166 (2009).

37. Ridgway, S. & Keady, J. J. The IRC +10216 circumstellar envelope. II - Spatial measurements of the dust. *ApJ* **326**, 843–858 (1988).

38. Keady, J. J. & Ridgway, S. T. The IRC + 10216 circumstellar envelope. III - Infrared molecular line profiles. *ApJ* **406**, 199–214 (1993).

39. De Beck, E. *et al.* Probing the mass-loss history of AGB and red supergiant stars from CO rotational line profiles. II. CO line survey of evolved stars: derivation of mass-loss rate formulae. *A&A* accepted for publication (2010).

40. Ladjal, D. *et al.* 870 μm observations of evolved stars with LABOCA. *A&A* **513**, A53 (2010).

41. Cherchneff, I., Glassgold, A. E. & Mamon, G. A. The formation of cyanopolyyne molecules in IRC + 10216. *ApJ* **410**, 188–201 (1993).

42. Men'shchikov, A. B., Balega, Y., Blöcker, T., Osterbart, R. & Weigelt, G. Structure and physical properties of the rapidly evolving dusty envelope of IRC +10 216 reconstructed by detailed two-dimensional radiative transfer modeling. *A&A* **368**, 497–526 (2001).

43. van Dishoeck, E. F., Jonkheid, B. & van Hemert, M. C. Photoprocesses in protoplanetary disks. *Chemical Evolution of the Universe, Faraday Discussions, volume 133, 2006, p.231* **133**, 231 (2006).

44. Woodall, J., Agúndez, M., Markwick-Kemper, A. J. & Millar, T. J. The UMIST database for astrochemistry 2006. *A&A* **466**, 1197–1204 (2007).

45. Draine, B. T. Photoelectric heating of interstellar gas. *ApJS* **36**, 595–619 (1978).

46. Agúndez, M. & Cernicharo, J. Oxygen Chemistry in the Circumstellar Envelope of the Carbon-Rich Star IRC +10216. *ApJ* **650**, 374–393 (2006).

47. Sahai, R. & Chronopoulos, C. K. The Astrosphere of the Asymptotic Giant Branch Star IRC+10216. *ApJ* **711**, L53–L56 (2010).

48. Conway, J., Elitzur, M. & Parra, R. Spectral line and continuum radiation propagation in a clumpy medium. *Ap&SS* **295**, 319 – 324 (2004).